Polymer 53 (2012) 5575–5581

Contents lists available at SciVerse ScienceDirect

Polymer

journal homepage: www.elsevier.com/locate/polymer

Mitigation of fatigue damage in self-healing vascular materials

A.R. Hamilton [a,b,1], N.R. Sottos [b,c,*], S.R. White [b,d]

[a] Department of Mechanical Science and Engineering, University of Illinois at Urbana-Champaign, 1206 W. Green St., 61801 Urbana, IL, United States
[b] Beckman Institute for Advanced Science and Technology, 405 N. Mathews Ave., 61801 Urbana, IL, United States
[c] Department of Materials Science and Engineering, University of Illinois at Urbana-Champaign, 1304 W. Green St., 61801 Urbana, IL, United States
[d] Department of Aerospace Engineering, University of Illinois at Urbana-Champaign, 104 S. Wright St., 61801 Urbana, IL, United States

ARTICLE INFO

Article history:
Received 20 June 2012
Received in revised form
19 September 2012
Accepted 23 September 2012
Available online 28 September 2012

Keywords:
Self-healing
Fatigue
Vascular network

ABSTRACT

The fatigue response of an epoxy matrix containing vasculature for the delivery of liquid healing agents is investigated. The release of a rapidly curing, two-part epoxy healing chemistry into the wake of a propagating crack reduces the rate of crack extension by shielding the crack tip from the full range of applied stress intensity factor. Crack propagation is studied for a variety of loading conditions, with the maximum applied stress intensity factor ranging from 62 to 84% of the quasi-static fracture toughness of the material. At the highest level of applied load, the rate of mechanical damage is so fast that the healing agents do not fully mix and polymerize, and the effect of healing is minimal. The self-healing response is most effective at impeding the slower propagating cracks, with complete crack arrest occurring at the lowest level of applied load, and reductions of 79–84% in the rate of crack extension at intermediate loads.

1. Introduction

Thermosetting polymers are susceptible to crack growth under repeated loading. The accumulation of damage degrades the mechanical performance and can lead to catastrophic failure of the material. Fatigue is particularly problematic because it occurs at stress levels below the critical fracture stress under quasi-static loading conditions [1]. One strategy to compensate for poor fatigue resistance is to provide a mechanism for recovery of mechanical integrity after damage. Self-healing materials accomplish this recovery without the external intervention usually associated with manual repair and maintenance. In general, healing involves forming or reforming bonds across a damaged region by one of several mechanisms, including the deployment of reactive liquid healing agents, or utilizing latent reactivity or reversible bonds within the matrix material [2].

Although several approaches to self-healing have successfully demonstrated the recovery of quasi-static mechanical properties, relatively few have been shown to advantageously affect damage propagation under fatigue loading conditions [3–8]. Brown et al. [3,4] demonstrated that a self-healing system consisting of a microencapsulated monomer and solid catalyst could impede or arrest the propagation of cracks under cyclic fatigue. The authors attributed retardation of crack extension to several crack-tip shielding mechanisms enabled by the self-healing constituents. The hydrodynamic pressure exerted by a viscous fluid (i.e. liquid healing agents) in the wake of a growing crack slows crack growth by resisting the motion of the crack faces [9–11]. This effect is enhanced when the fluid viscosity is increased, the range of applied stress intensity factor (ΔK) is reduced, the frequency (f) is increased, or the specimen thickness is increased. In self-healing materials, hydrodynamic shielding increases as liquid healing agents polymerize and increase in viscosity. Crack bridging by solid polymer formed in the damage zone serves as another shielding mechanism that extends fatigue lifetime, although this mechanism is reportedly short-lived due to rapid propagation through the healed material. After failure of the adhesive bond between the crack faces, the remaining healed material continues to shield the crack tip by acting as a wedge that prevents complete crack closure. The effects of crack closure contribute more significantly than crack bridging to the fatigue life extension observed for self-healing materials [3–5]. Each of these mechanisms act to shield the crack tip from the full range of the applied stress intensity factor (ΔK), resulting in a reduction of the rate of crack propagation in accordance with the Paris power law [12]:

* Corresponding author. Beckman Institute for Advanced Science and Technology, 405 N. Mathews Ave., 61801 Urbana, IL, United States. Tel.: +1 217 333 1041; fax: +1 217 333 2736.
E-mail address: n-sottos@illinois.edu (N.R. Sottos).
[1] Present address: School of Mechanical and Aerospace Engineering, Queen's University Belfast, Ashby Building, Stranmillis Road, Belfast BT9 5AH, United Kingdom.

0032-3861/$ – see front matter © 2012 Elsevier Ltd. All rights reserved.
http://dx.doi.org/10.1016/j.polymer.2012.09.050

$$\frac{da}{dN} = C_0 \Delta K_I^n, \quad (1)$$

where a is crack length, N is the number of load cycles applied, da/dN is the rate of crack propagation, ΔK_I is the range of the mode I stress intensity factor, and C_0 and n are parameters that depend upon the material and the loading conditions—including the frequency (f), and stress intensity ratio ($R = K_{min}/K_{max}$).

Jones et al. [5] showed that further reduction in the fatigue crack growth rate is possible in microcapsule-based self-healing materials by employing healing agents with faster chemical kinetics. These faster-reacting healing agents provided more fatigue lifetime extension under a given set of loading conditions than previous self-healing systems because the rate of healing agent polymerization increased relative to the rate of crack propagation. Whereas previous studies by Brown et al. reported arrest of crack growth when $K_{max} = 0.30K_{IC}$, and retardation of crack growth up to $K_{max} < 0.45K_{IC}$, Jones et al. achieved arrest of faster-growing cracks when loading to $K_{max} = 0.45K_{IC}$, and impeded crack growth up to $K_{max} < 0.62K_{IC}$ using healing agents that polymerize four times faster. These rapidly curing healing agents have a gel time of less than 10 min, and resulted in specimen lifetime extension by as much as 6.7 times beyond the 20.2 h lifetime of equivalent non-healing specimens.

Microcapsule-based self-healing materials are inherently limited in the volume of healing agents available for repair of damage, which is determined by the size and concentration of microcapsules distributed within the matrix material [13]. An alternative mode of healing agent delivery that overcomes this limitation was proposed by Toohey et al. [14], in which a vascular system of interconnected microchannels (ca. 200 μm in diameter) distributes healing agents throughout the material. Compared to microcapsule-based materials, this vascular approach provides a continuous supply of healing agents, enabling repeated healing events within a given region of material and the possibility of infiltrating larger damage volumes. Vascular systems have been embedded within an epoxy substrate to heal cracks in coating materials [15,16], within foam core materials to heal impact damage in composite sandwich structures [17,18], and within bulk epoxy to heal damage within the vascular material itself [19]. Three-dimensional vascular systems have been introduced into woven fiber-reinforced composites to impart a range of functionality [20]. Other studies have demonstrated the integration of segregated vasculature into fiber-reinforced laminates, evaluated the effect on mechanical integrity [21–25] and reported the first steps toward vascular based self-healing of these composites [26].

In this study, a self-healing vascularized epoxy is subjected to crack growth under cyclic loading. External pumps are utilized to provide a continuous supply of two liquid healing agents, which were selected for their rapid gel time. The effect of healing agent delivery and polymerization of the healing agent is explored under a range of applied load amplitudes, and healing agent pumping rates.

2. Experimental

Crack propagation under fatigue loading was investigated using the double cleavage drilled compression (DCDC) fracture sample geometry, shown in Fig. 1. Upon application of a compressive load, tensile stresses develop at the top and bottom of the hole, driving the propagation of precracks at these locations. An analysis of the sample geometry [27] predicts that the nominal applied stress required for crack propagation is independent of crack length after sufficient crack extension (approximately $a/R > 1.5$ for the dimensions and epoxy material used in this study).

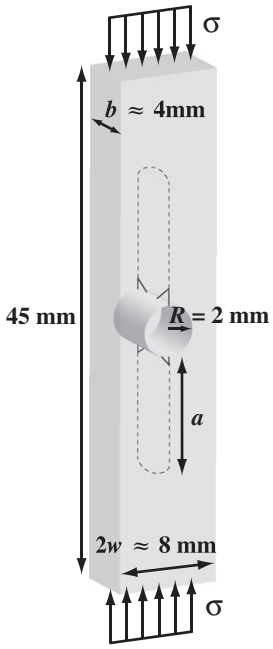

Fig. 1. Schematic of DCDC fracture sample geometry. Precrack locations are shown as solid lines and the expected crack path is shown as dashed lines.

Vascular DCDC specimens were manufactured with two microchannels located on each half of the sample, positioned a distance of 5 mm from the central hole, as shown in Fig. 2. Specimens were created by pouring a degassed mixture of Epon 828 epoxy resin (DGEBA) and 40 pph Epikure 3274 curing agent (aliphatic amine) into rubber molds. Microchannels were created by placing nylon fibers 230 μm in diameter at the desired locations in the mold, and extracting them from the specimens, post-cure. Specimens were cured for 24 h at room temperature (20–23 °C) and a controlled humidity (20–25% relative humidity), followed

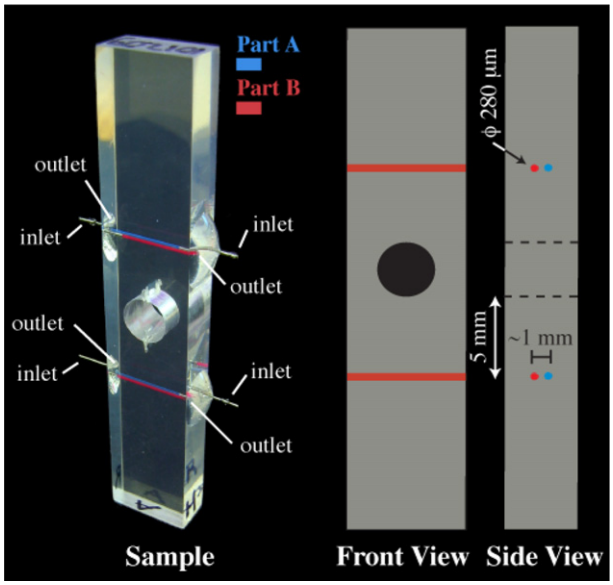

Fig. 2. Image (left) and schematic drawings (right) of a vascular DCDC specimen with microchannels containing Part A (shown in red), and Part B (shown in blue) of the two-part epoxy healing chemistry. (For interpretation of the references to color in this figure legend, the reader is referred to the web version of this article.)

by 48 h in an oven at 30 °C. At least 7 additional days of cure time at room temperature elapsed before samples were tested. Further cure time beyond this minimum was not found to have a significant impact on fatigue crack propagation. The critical stress intensity factor (K_{IC}) of this material is 0.59 ± 0.01 MPa $m^{1/2}$, as determined by quasi-static fracture tests.

Each microchannel contained one component (Part A or Part B) of a commercially available two-part epoxy adhesive (ITW Devcon High Strength 5 Minute® Epoxy), which was selected for its rapid cure kinetics and recommended mix ratio of 1:1. External reservoirs of each healing agent were supplied to the corresponding microchannels using flexible PVC tubing (Thermo Scientific Nalgene®), Luer adapters with barbed fittings, and 32 gauge (100 μm inside diameter, 240 μm outside diameter) stainless steel dispensing tips (Nordson EFD, Inc.) inserted approximately 1–3 mm into the microchannels. Microchannel outlets were left open to atmospheric pressure, allowing healing agents to flow either through the microchannel or into the damage zone (after the microchannels were ruptured by intersecting cracks).

2.1. Pumping protocol

Constant and equal flow rates of the two healing agents were delivered using a positive displacement syringe pump (KD Scientific Model 210P). The stroke of the pump resulted in displacement of fluid from the syringes at specified flow rates, but actual flow rates were not directly measured at the microchannel inlets or at the points of access to the damage zone. In order to estimate the actual flow rates into the damage zone, calibration tests were conducted in which healing agents were pumped through the same system of tubing and dispensing tips and the mass of fluid pumped was recorded as a function of time (see the supplementary data for more detail). The calibrations revealed that, although the pumping rates were equal, the actual flow rate of Part B was approximately 60% lower than the flow rate of Part A, due to the higher viscosity of Part B. In this manuscript, the specified pumping rate is used to refer to the various testing conditions, rather than the estimated actual flow rate of each healing agent.

2.2. Mechanical testing

Notches were scored at the locations shown in Fig. 1 using a razor, and precracks were initiated by pre-test cycling (under the same conditions as the subsequent fatigue test) until cracks extended 2 mm from the central hole. Fatigue tests were conducted on an Instron DynoMight 8841 hydraulic load frame with a 1 kN load cell. A triangular waveform (Fig. 3) was applied at a frequency of 2 Hz and a stress intensity ratio (R) of 0.1. A range of maximum stress intensity factors (K_{max}) was applied from 62 to 84% of the quasi-static fracture toughness (0.62–0.84K_{IC}) of the material. Optical measurements of crack extension were obtained from images captured at regular intervals by a CCD camera. Fatigue tests were stopped after cracks had extended approximately 10 mm from the central hole. After testing, each microchannel was assessed for obstructions to determine whether the supply of healing agents had been maintained. Microchannel blockage was determined by injecting ethanol via a syringe fitted with a dispensing tip inserted into the microchannel; if the flow of ethanol through the microchannels was not detected, then they were considered blocked.

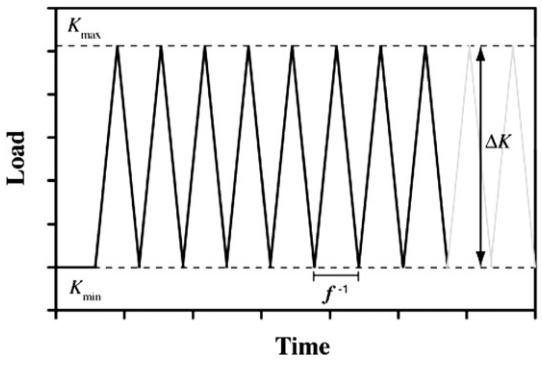

Fig. 3. Triangular load waveform, showing relevant fatigue loading parameters.

2.3. Quantifying healing effect

The effect of healing agent delivery to cracks in self-healing samples was quantified using the life extension ratio, λ, introduced by Brown et al. [3],

$$\lambda = \frac{N_{healed} - N_{control}}{N_{control}}, \tag{2}$$

where N_{healed} is the lifetime in cycles of a vascular specimen, and $N_{control}$ is the lifetime of a plain epoxy specimen under the same load conditions. Lifetimes were determined as the number of cycles elapsed for crack extension from a length of 5 mm (the location of the microchannels) to a final length of 10 mm.

The crack growth rate reduction ratio, ψ, was defined as a second measure of the effect of healing agents based on the rate of crack propagation,

$$\psi = 1 - \frac{(da/dN)_{healed}}{(da/dN)_{control}}, \tag{3}$$

where $(da/dN)_{healed}$ and $(da/dN)_{control}$ are the rates of crack propagation in a self-healing specimen and a plain epoxy specimen, respectively. Crack growth rates were determined using a linear regression analysis of crack length data in the range of a = 5–10 mm. A value of $\psi = 0$ signifies that healing had no effect on the rate of crack propagation compared with the control samples and $\psi = 1$ signifies complete crack arrest.

3. Results and discussion

3.1. Healing agent chemistry

The chemical kinetics of the healing agent chemistry were characterized by dynamic scanning calorimetry (DSC) and dynamic mechanical analysis (DMA). The degree of cure (α) was calculated as

$$\alpha(t) = \frac{H(t)}{H_R}, \tag{4}$$

where $H(t)$ is the enthalpy of reaction up to time t, and H_R is the total enthalpy of reaction. $H(t)$ was obtained from an isothermal DSC scan performed at room temperature, and H_R was determined by a dynamic scan from 25 to 300 °C. Degree of cure is plotted as a function of time at room temperature (T = 25 °C) in Fig. 4(a). After about 10 min the degree of cure started to plateau at approximately 77%.

The evolution of the storage and loss moduli in compression was determined as a function of cure time using a DMA (TA Instruments RSA3) with parallel plate fixtures. Cylindrical samples of the healing material—7 mm in diameter and 4 mm thick—were tested at regular intervals during the initial hours following polymerization.

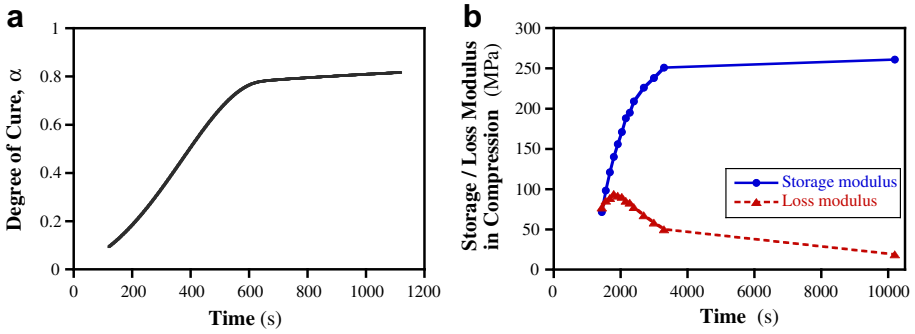

Fig. 4. (a) Degree of cure and (b) development of compressive storage and loss moduli of ITW Devcon High Strength 5 Minute® epoxy as a function of cure time at room temperature (25 °C).

The resulting curves are presented in Fig. 4(b). After 20 min the material was sufficiently solidified to demold and test, and after 55 min the storage modulus began to plateau at approximately 250 MPa. The dynamic viscosities of each healing agent (Part A and Part B) were measured on a rheometer (TA Instruments AR-G2) with parallel plate fixtures, and are given in Table 1.

3.2. Fatigue of epoxy specimens

With the frequency (f) and load ratio (R) held constant, the rate of crack propagation in the epoxy matrix material, shown in Fig. 5, was adequately described by the Paris power law (Equation (1)). Crack growth rates were determined using a linear regression analysis of the crack length data in the range $5 < a < 10$ mm. The Paris law parameters, as determined by a least squares linear fit to the data in Fig. 5, are given in Table 2.

3.3. Self-healing specimens at $K_{max} = 0.73K_{IC}$

Representative plots of crack length evolution are shown in Fig. 6 for plain epoxy and vascular specimens loaded to $K_{max} = 0.73K_{IC}$. All specimens exhibited approximately the same crack growth rates in the region of material before the microchannel locations ($a < 5$ mm). Cracks in plain epoxy specimens (Fig. 6, curve ①) propagated at a nominally constant rate owing to the crack length independent behavior of the DCDC specimen geometry. Vascular samples without any fluid in the microchannels (Fig. 6, curve ②) behaved similarly to plain epoxy samples.

After cracks intersected fluid-filled microchannels (Fig. 6, curves ③–⑤), healing agents flowed into the crack plane and the rate of crack propagation decreased. Curve ③ is representative of the fatigue behavior of specimens in which only one healing agent (either Part A, or Part B) was supplied to the microchannels at rates ranging from 1 to 4 μL/h (the flow rate did not appreciably affect the rates of crack propagation). Even though no polymerization occurred in the crack plane, there was a significant decrease in da/dN and increase in the fatigue life, which can be attributed to crack tip shielding due to hydrodynamic pressure. Using Equation (1) along with the parameters given in Table 2 and based on the reduced rate of crack propagation (da/dN), the effective maximum stress intensity at the crack tip was estimated as $(K_{max})_{effective} \approx 0.39$ MPa $m^{1/2} \approx 0.92(K_{max})_{applied}$ for specimens with just one healing agent supplied to the crack. The insensitivity of the crack growth rate to the different viscosities of the healing agents (reported in Table 1) is consistent with existing models of hydrodynamic shielding. These models predict a decrease in the amplitude of the effective stress intensity factor with increasing viscosity until reaching a threshold at approximately 10^{-3} Pa s. After this point, only an order of magnitude difference in viscosity above this threshold value will lead to any appreciable change in crack growth rate [10]. The healing agent pumping rate also did not affect hydrodynamic shielding because the pumping pressure (approximately 10^{-1} MPa, assuming Poiseuille flow) was negligible compared with the hydrodynamic pressures associated with dynamic loading of fluid in the crack (on the order of 10^{1} MPa [11]).

Curve ④ is representative of specimens with both healing agents pumped at a constant rate of 2 μL/h or less. After crack extension to 10 mm, these specimens consistently had one or more obstructed microchannels. When healing agents were pumped at a rate of 4 μL/h or more, fluid flow remained unobstructed for the duration of the tests, and fatigue crack growth was further retarded (curve ⑤). Interestingly, the specimen in curve ⑤ exhibited a transition to a lower crack growth rate at a crack length of approximately 7.5–8 mm, which did not correspond to any obvious feature in the specimen at this location. This transition to a lower growth rate was observed in all self-healing specimens loaded to $K_{max} \leq 0.73K_{IC}$. The larger crack opening displacements associated with longer crack lengths may account for this decreased rate of propagation by

Table 1
Dynamic viscosities of ITW Devcon High Strength 5 Minute® epoxy self-healing chemistry.

Component	Viscosity (Pa s)
Part A	15.8
Part B	20.1

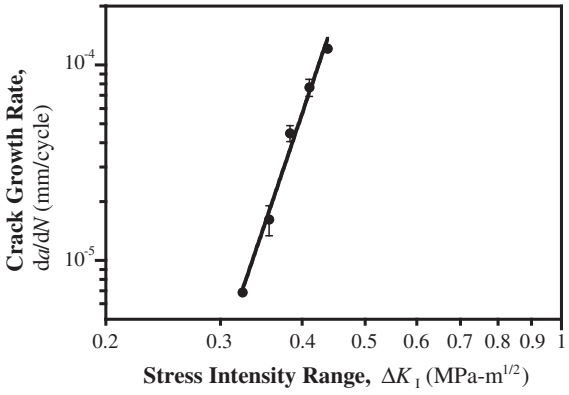

Fig. 5. Crack growth rate as a function of applied stress intensity range in plain epoxy specimens. Experimental data are shown as black circles, and the best-fit Paris power law prediction as solid black line. Data with error bars represent an average of three specimens. Error bars bound one standard deviation.

Table 2
Paris power law parameters for plain epoxy (Epon 828/Epikure 3274) specimens.

C_0	n
0.461	9.84

facilitating healing agent flow into the damage zone (see Supplementary Data for further discussion of this hypothesis). The effective stress intensity at the crack tip in specimens with both healing agents delivered to the damage zone was estimated as $(K_{max})_{effective} \approx 0.38$ MPa $m^{1/2} \approx 0.88(K_{max})_{applied}$ for specimens with low pumping rates (<2 μL/h), and $(K_{max})_{effective} \approx 0.36$ MPa $m^{1/2} \approx 0.85(K_{max})_{applied}$ for specimens with high pumping rates (4–7 μL/h).

Representative fracture surfaces of specimens with one or both healing agents present in the vascular system are shown in Fig. 7 after crack extension to approximately 10 mm and cyclic loading to $K_{max} = 0.73K_{IC}$. Unreacted healing agents in the damage zone were removed before imaging by flushing the crack with ethanol and gently wiping the surface. The fracture surfaces of specimens with only Part A or only Part B supplied to the crack plane contained no healed material in the crack plane (Fig. 7(a)), confirming that the prolonged fatigue life of these control samples was due to hydrodynamic pressure crack-tip shielding. In contrast, the fracture surfaces of specimens in which both healing agents were supplied to the crack plane (Fig. 7(b)–(d)) exhibited a polymer film formed by the reaction of the two healing agents. Consequently, the extended fatigue life of these specimens can be attributed to the reaction of the healing agents, which increased the viscosity of the fluids in the crack plane (enhancing hydrodynamic shielding), and led to the formation of a solid wedge that provided crack closure shielding to the crack tip.

Samples with low pumping rates (<2 μL/h) and obstructed microchannels by the end of testing had the least healed material coverage in the crack plane (Fig. 7(b)), due to blocked microchannels causing a lack of one of both healing agents in the crack plane during testing. Microchannel blockages may have formed below a critical flow rate as a result of polymerization over the microchannel inlet into the crack plane, or polymerization in the microchannels as hydrodynamic pressure in the damage zone forced healing agents back into the microchannels.

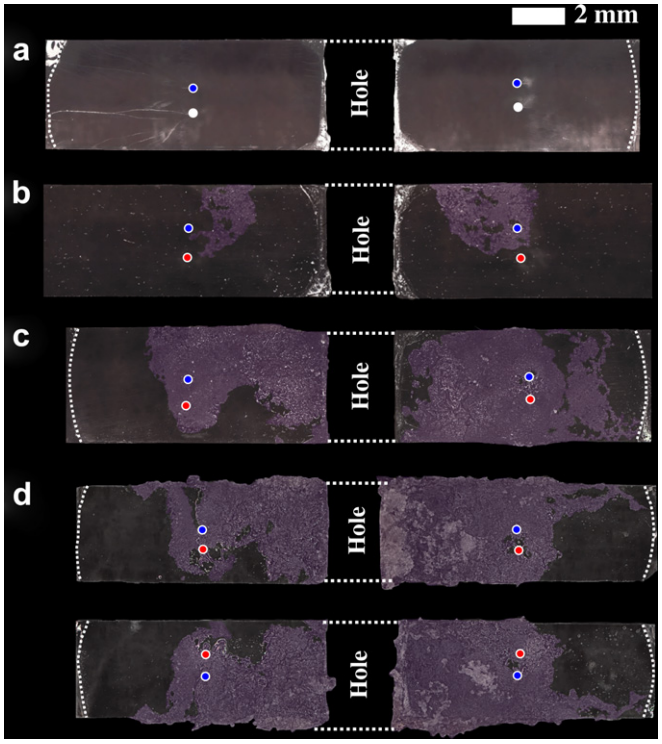

Fig. 7. Fracture surfaces of specimens loaded to $K_{max} = 0.73K_{IC}$ with (a) a single healing agent delivered to the cracks, (b) both healing agents delivered at a low pumping rate (such that the microchannels became clogged), (c) both healing agents delivered at 4 μL/h (flow maintained throughout testing), (d) both healing agents delivered at 7 μL/h (flow maintained throughout testing). Healed material is highlighted in false purple coloring. Microchannels are highlighted with solid circles colored red for those containing Part A, blue for those containing Part B, or white for empty channels. (For interpretation of the references to color in this figure legend, the reader is referred to the web version of this article.)

Samples with high pumping rates (4 μL/h) had more polymer coverage in the crack plane (Fig. 7(c)), although coverage was incomplete (final crack-tip positions are indicated with dashed lines). This lack of complete coverage indicates that the healing agents could not access all areas of the crack plane or the mixing of the two fluids was insufficient to initiate polymerization at certain locations in the crack. In all cases, polymer formation was biased to the side of the

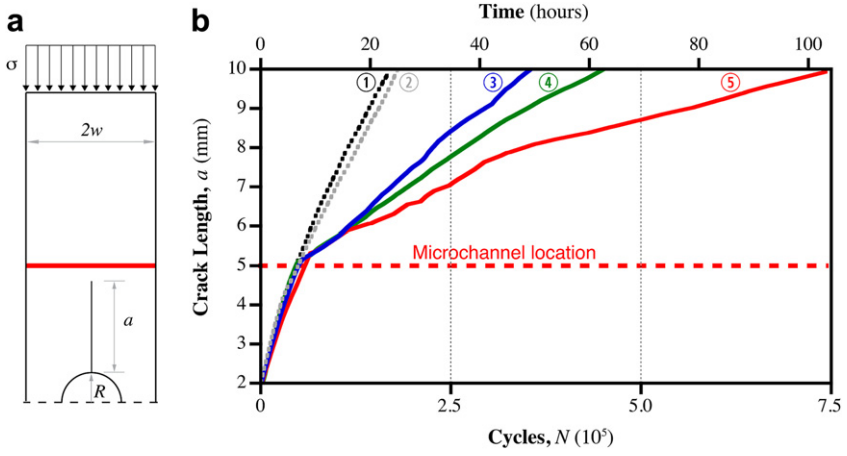

Fig. 6. (a) Schematic of DCDC sample showing relevant quantities and microchannel location (dashed line). (b) Representative plots of crack length as a function of time in ① a plain epoxy and ② vascular specimens containing no healing agents, ③ vascular specimens containing one healing agent, and vascular specimens with both healing agents pumped at a rate of ④ <2 mL/h (obstructed), and ⑤ 4–7 mL/h (unobstructed). All specimens loaded to $K_{max} = 0.73K_{IC} = 0.43$ MPa $m^{1/2}$.

crack plane where Part B was delivered (microchannels containing Part B are highlighted blue in Fig. 7), indicating that the availability of Part B in the damage zone was the limiting factor to more extensive healed material formation. The lack of Part B in the damage zone was likely caused by its higher viscosity (limiting mobility in the crack plane), and by the lower effective flow rates relative to Part A (see Pumping Protocols in the Experimental section).

The fracture surfaces on both halves of a specimen in which the healing agent pumping rate was 7 μL/h are shown in Fig. 7(d). Polymer film formed on the same locations of the two matching faces of the crack plane, indicating adhesive failure of the healed material and that crack bridging was an active mechanism shielding the stress intensity factor at the crack tip. Comparison of the crack planes in Fig. 7(c) and (d), reveals that increasing the pumping rate from 4 to 7 μL/h resulted in more polymer formation in the crack plane, with additional healed material concentrated in the region between the crack root ($a = 0$) and the microchannel locations ($a = 5$). The fatigue performance and lifetimes of these two samples were approximately the same (as compared in Fig. 8), indicating that the additional healed material formed in the specimen pumped at 7 μL/h had little effect on crack propagation.

3.4. Self-healing specimens at $K_{max} = 0.62K_{IC}$

Crack propagation was completely arrested by the constant pumping of both healing agents into specimens loaded at a load of $K_{max} = 0.62K_{IC}$. Crack evolution is plotted in Fig. 9 for plain epoxy specimens (curve ⑦) and vascular specimens with healing agents delivered at a rate of 7 μL/h (curve ⑧). The microchannels in this self-healing specimen were unobstructed at the end of testing. Cyclic loading was continued for approximately 5 days after crack propagation in the self-healing sample reached an endurance limit, after which time the crack was considered arrested and the test was halted. Crack arrest did not occur immediately after healing agent release (at $a = 5$ mm), but rather after further crack extension to about 8 mm. This same tendency for crack growth to slow after propagation beyond the microchannel locations was also observed in specimens loaded to $K_{max} = 0.73K_{IC}$ (curve ⑤ in Fig. 6), indicating that the same cause is likely responsible for the reduced rate of crack propagation under both loading conditions.

3.5. Fatigue behavior at various load amplitudes

Healing efficiency in terms of crack propagation rates (ψ) and sample lifetimes (λ) is summarized in Fig. 10 for the different levels

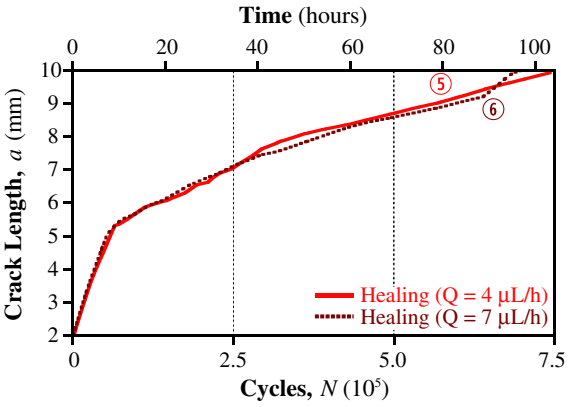

Fig. 8. Crack length as a function of time in vascular specimens with healing agents pumped at constant rates of ⑤ 4 and ⑥ 7 μL/h (unobstructed). Specimens were loaded to $K_{max} = 0.73K_{IC} = 0.43$ MPa $m^{1/2}$.

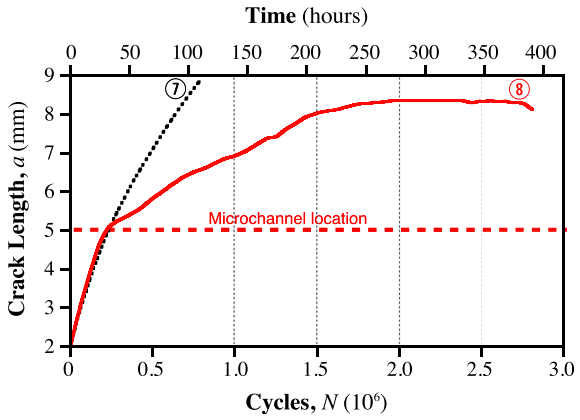

Fig. 9. Crack length as a function of time in ⑦ plain epoxy, ⑧ vascular specimens with both healing agents pumped at 7 μL/h (unobstructed). Both specimens were loaded to $K_{max} = 0.62K_{IC} = 0.38$ MPa $m^{1/2}$.

of applied load, and in specimens with one or both healing agents supplied. The number of samples tested is indicated at each point, and average values are plotted whenever more than one sample was tested. Error bars are not shown because the standard deviation from the mean was less than 2% in all cases. Samples with constant, unobstructed pumping of healing agents were tested at maximum applied stress intensities of $K_{max} = 0.62K_{IC}$, $0.73K_{IC}$, $0.78K_{IC}$, and $0.84K_{IC}$ (crack length data as a function of time for

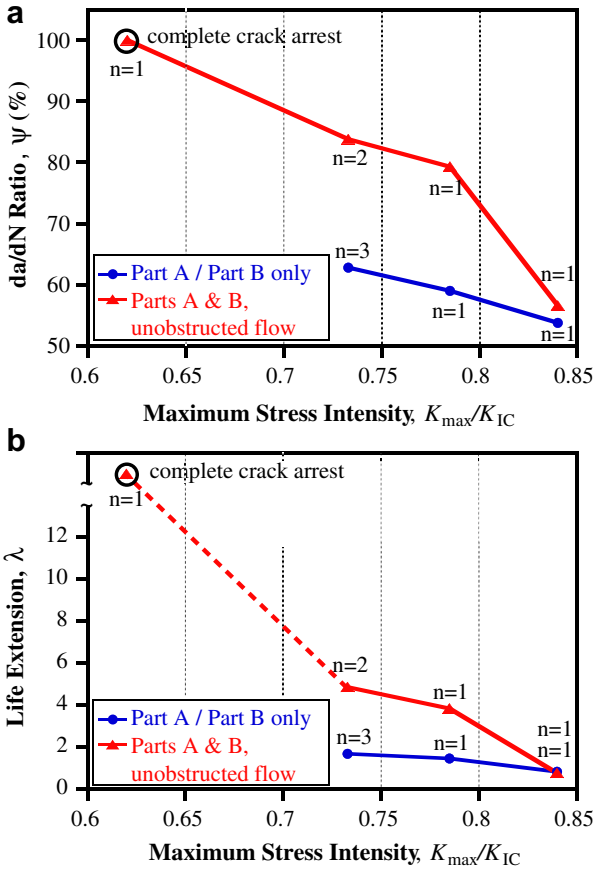

Fig. 10. Effect of healing agents on (a) the crack growth rate and (b) the sample lifetime. The number of specimens tested is specified next to each point. In the case of complete crack arrest, ψ was plotted as 100%, rather than calculated using Equation (3).

samples loaded to $K_{max} = 0.78K_{IC}$ and $K_{max} = 0.84K_{IC}$ are given as supplementary data).

Complete crack arrest occurred at $K_{max} = 0.62K_{IC}$. In general, healing performance decreased (in terms of both ψ and λ) as the maximum applied stress (K_{max}) increased. For $K_{max} = 0.73K_{IC}$, life extension reduced to $\psi = 84\%$ and $\lambda = 4.9$, with similar trends for $K_{max} = 0.78K_{IC}$, $\psi = 79\%$ and $\lambda = 3.8$, and at $K_{max} = 0.84K_{IC}$, $\psi = 55\%$ and $\lambda = 0.8$. Although the critical pumping rates to prevent microchannel blockage were not precisely determined under each loading condition, the values generally increased with an increase in the applied load and ranged from 4 μL/h at $K_{max} = 0.73K_{IC}$ to 10 μL/h at $K_{max} = 0.84K_{IC}$. The downward slope in Fig. 10 for specimens with only one healing agent (Part A/B only) indicates that the effect of hydrodynamic pressure decreased with an increase in the maximum applied stress intensity, as expected. At the highest maximum applied stress level ($K_{max} = 0.84K_{IC}$) the healing performance of specimens with only one healing agent and specimens with both healing agents converge, indicating that the only crack-tip shielding mechanism affecting crack propagation in these samples was hydrodynamic pressure; healing agent mixing and polymerization were too slow to affect the rapid propagation of damage under these loading conditions.

4. Conclusion

Fatigue crack growth in an epoxy matrix was impeded by infiltrating the cracks with liquid healing agents via a simple vascular system consisting of two microchannels and external pumps. The presence of a viscous fluid in the crack plane reduced the rate of crack propagation through a hydrodynamic pressure crack-tip shielding mechanism. Healed material formed in the crack plane from the polymerization of the healing agents further reduced the rate of crack propagation through adhesion between the crack faces and crack-closure. The effect of healing agent delivery on fatigue behavior was quantified in terms of both the fatigue lifetime of the specimens (λ) and the crack growth rate (ψ). In the most rapidly propagating cracks, the shielding mechanisms due to healing agent polymerization were absent and only hydrodynamic pressure affected crack propagation rate. Slower propagating cracks benefitted from an additional reduction in the rate of crack propagation when both healing agents were supplied and a polymer film was formed in the damage zone. A critical pumping rate was required to prevent microchannels from clogging, which was dependent upon the amplitude of the applied load. Compared to previous studies of microcapsule-based self-healing materials subjected to fracture under fatigue, crack arrest and retardation was achieved at higher levels of applied maximum stress intensity (K_{max}/K_{IC}) using this vascular self-healing system. Recent studies into vascular self-healing suggest that further improvements may be obtained by implementing healing agent mixing strategies [28]. Optimizing vascular system design and healing agent chemistry offer further opportunities for improvement of fatigue characteristics.

Acknowledgments

This work was supported by the Air Force Office of Scientific Research Multidisciplinary University Research Initiative (grant F49550-05-1-0346). The authors would like to thank their colleagues in the Autonomous Materials Systems Research group at the Beckman Institute for Advanced Science and Technology.

Appendix A. Supplementary material

Supplementary material associated with this article can be found, in the online version, at http://dx.doi.org/10.1016/j.polymer.2012.09.050.

References

[1] Sauer JA, Richardson GC. Int J Fract 1980;16(6):499–532.
[2] Blaiszik BA, Kramer SLB, Olugebefola SC, Moore JS, Sottos NR, White SR. Annu Rev Mater Res 2010;40:179–211.
[3] Brown EN, White SR, Sottos NR. Compos Sci Technol 2005;65:2466–73.
[4] Brown EN, White SR, Sottos NR. Compos Sci Technol 2005;65:2474–80.
[5] Jones AS, Rule JD, Moore JS, Sottos NR, White SR. J R Soc Interf 2007;4:395–403.
[6] Keller MW, White SR, Sottos NR. Polymer 2008;49(13–14):3136–45.
[7] Jin H, Miller GM, Sottos NR, White SR. Polymer 2011;52(7):1628–34.
[8] Zako M, Takano N. J Intell Mater Syst Struct 1999;10(10):836–41.
[9] Tzou JL, Suresh S, Ritchie RO. Acta Metall 1985;33(1):105–16.
[10] Tzou JL, Hsueh CH, Evans AG, Ritchie RO. Acta Metall 1985;33(1):117–27.
[11] Yi KS, Cox BN, Dauskardt RH. J Mech Phys Solid 1999;47(9):1843–71.
[12] Paris PC, Gomez MP, Anderson WE. Trend Eng Univ Wash 1961;13(1):9–14.
[13] Rule JD, Sottos NR, White SR. Polymer 2007;48:3520–9.
[14] Toohey KS, Sottos NR, Lewis JA, Moore JS, White SR. Nat Mater 2007;6:581–5.
[15] Toohey KS, Hansen CJ, Lewis JA, White SR, Sottos NR. Adv Funct Mater 2009;19(9):1399–405.
[16] Hansen CJ, Wu W, Toohey KS, Sottos NR, White SR, Lewis JA. Adv Mater 2009;21:1–5.
[17] Williams HR, Trask RS, Bond IP. Compos Sci Technol 2008;68:3171–7.
[18] Williams HR, Trask RS, Bond IP. Smart Mater Struct 2007;16:1198–207.
[19] Hamilton AR, Sottos NR, White SR. Adv Mater 2010;22:5159–63.
[20] Esser-Kahn AP, Thakre PR, Dong H, Patrick JF, Vlasko-Vlasov VK, Sottos NR, et al. Adv Mater 2011;23(32):3654–8.
[21] Norris CJ, Trask RS, Bond IP. Compos Sci Technol 2011;71:847–53.
[22] Norris CJ, Trask RS, Bond IP. Composites, Part A 2011;42:639–48.
[23] Huang C, Trask RS, Bond IP. J R Soc Interf 2010;49:1229–41.
[24] Trask RS, Bond IP. J R Soc Interf 2010;47:921–31.
[25] Phillips DM, Pierce MR, Baur JW. Composites, Part A 2011;42:1609–19.
[26] Norris CJ, Meadway G, O'Sullivan M, Bond IP, Trask RS. Adv Funct Mater 2011;21:3624–33.
[27] Plaisted TA, Amirkhizi AV, Nemat-Nasser S. Int J Fract 2006;141:447–57.
[28] Hamilton AR, Sottos NR, White SR. J R Soc Interf 2012;9:1020–8.